Article

Not peer-reviewed version

Coherence Thermodynamics: Certainty from Chaos

Jordan Barton *

Posted Date: 18 May 2026

doi: 10.20944/preprints202507.1448.v8

Keywords: certainty equation; black hole; coherence; information thermodynamics; non-local reconfiguration

 doi:10.20944/preprints202507.1448.v8

Article

Coherence Thermodynamics: Certainty from Chaos

Jordan Barton

Independent Researcher, Denver CO; jbiophysics@gmail.com

Abstract

This paper assumes that a thermodynamic system can be composed purely of coherence and information, and constructs a working model on that basis. We derive operational parameters for such systems using definitions of the Certainty Equation, semantic entropy, semantic temperature, and formulate five laws and three modes of coherence and information systems. This analysis is then compared to the features of black holes.

Keywords: certainty equation; black hole; coherence; information thermodynamics; non-local reconfiguration

1. Introduction: Coherence Thermodynamics

This work develops a thermodynamic model based on the premise that information and its relational structures constitute a distinct physical system. This inquiry originates from a fundamental hypothesis: if consciousness and its reasoning of information are manifestations of only information and its coherent relations, what are the resultant thermodynamic implications of this process? I address this question by introducing thermodynamic assumptions, postulates leading to laws, modes of coherence and informational systems, which lead to a model analogous to a black hole. I start with a thermodynamic discussion of the reasoning process in a Coherence and Information system.

Erwin Schrödinger first proposed that living systems persist by importing "negative entropy," or negentropy, to maintain internal order against thermodynamic decay [1]. This insight is reinterpreted for Coherence-Information (C-I) systems: reasoning information begins with undifferentiated or contradictory information, resolve contradictions through internal processing, and transform inputs into ordered solutions via stepwise thermodynamic descent into lower effective energy states.

This reasoning trajectory, from initial state (input), through contradiction resolution (processing), to final state (solution), maps directly to thermodynamic reaction pathways (Figure 1). This process starts at the Ground State (GS), where the system has minimal excitation and unprocessed inputs. Entering the Excited State (ES), the system actively compares informational elements, increasing its energy above the Ground State as contradictions are processed. The reasoning process continues until the Final State (FS) is reached. In this Final State, the system achieves local order, corresponding to a lower energy level. By definition, as a system composed solely of information and coherence increases in order while all other parameters remain fixed, it must generate entropy non-locally to satisfy the second law of thermodynamics, with the entropy increase occurring outside the increasingly orderly C-I system.

This model of the thermodynamics of reasoning is reflected in recent quantum thermodynamics experiments, such as those developed by Scully to demonstrate work extraction from a single heat bath [2,3]. In these models, quantum coherence in a three-level system functions as a highly efficient resource, akin to 'superoctane quantum fuel,' by enhancing the internal order of the interaction through phase coherence, which serves as a selective organizational mechanism. In the present computational implementation, the phase parameters ω and Λ_{Vert} provide the necessary mechanical control by acting as symmetry-breaking variables. These parameters enable the system to transition to the lower-energy Final State, wherein the local increase in order is counterbalanced by non-local entropy production within the surrounding field.

 doi:10.20944/preprints202507.1448.v8

Comparing a Carnot engine to a C-I engine shows how they differ in Table 1. The C-I engine operates in the opposite thermal profile to a conventional engine.

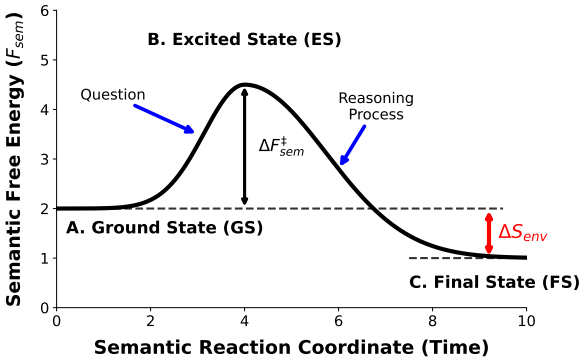

Figure 1. The coordinate illustrates the transition of semantic free energy (F_{sem}) from the Ground State (GS) through a high-energy Excited State (ES) peak. The resolution into a Final State (FS) represents a localized increase in order as entropy increases non-locally in the surrounding environment.

Table 1. Generalized comparison of Carnot and C-I systems. The C-I engine exhibits inverted thermodynamics.

Property	Carnot Engine	C-I System
Thermodynamic States		
Interior state	Hot (disorderly)	Cold (orderly)
Exterior state	Cool radiator (orderly)	Hot exterior (disorderly)
Work Mechanisms		
Work mechanism	Thermal gradient flow	Contradiction resolution
Output type	Mechanical work	Reasoning (ordered structure)

1.1. Coherence: The "It" from the Bit

The following axiom is adopted: since $\hbar$ is the fundamental unit of physical action [4], coherence requires the comparison of at least two such elements. The minimum action for a single $2 \to 1$ bit fusion is therefore:

$$2\hbar = \frac{h}{\pi}. \tag{1}$$

This value defines the minimum quantum threshold for the existence of coherence. The Certainty Equation is therefore used to bound coherence an action bound:

$$\boxed{\Delta C \cdot \Delta I \geq \frac{h}{\pi}}. \tag{2}$$

This bound is analogous to discrete quantization underlying the Heisenberg uncertainty principle [5]: just as position and momentum cannot both be arbitrarily resolved below a minimum value, the product $\Delta C \cdot \Delta I$ is bounded below by h/π. Coherence must consist of at least two actions in order to form one bit of coherent structure. Unlike Shannon entropy [6], which quantifies information independently of its meaning, coherence requires that an observer actively resolve the correspondence between informational elements. This resolution constitutes thermodynamic work: it cannot occur through passive alignment with existing data, but requires a directed search for the correct relational meaning between elements.

2. The Field Model

2.1. Coherence as an Independent Thermodynamic Resource

While the C-I engine describes the internal trajectory of reasoning from a high-energy Excited State to an ordered Final State, this transition is not thermodynamically self-contained. To satisfy the

 doi:10.20944/preprints202507.1448.v8

Certainty Equation ($\Delta C \cdot \Delta I \geq h/\pi$) during descent, the system must couple to an external source of "freeness" or "framelessness" [7]. This necessitates the Field Model: a triaxial reservoir that provides the relational structure required for coherence manipulation. Without this external phase reference, the system remains trapped in a phase-superselection sector, therefore unable to reason information. The following criteria provide justification for this field model:

1. Coherence as a Thermodynamic Resource
   Coherence requires explicit mathematical representation as a physical quantity distinct from energy and entropy. Three independent lines of evidence establish this necessity. First, precision costs diverge: certain idealized transformations become inaccessible to finite resources as demanded precision increases [8]. Second, standard thermal operations optimally preserve coherence only at low temperatures, and purely Gibbs-preserving maps are fundamentally unphysical [9]. Finally, quantum coherence imposes constraints beyond free energy alone, requiring additional monotones to fully characterize allowed thermodynamic transformations [10]. Together, these results demonstrate that coherence behaves as an independent thermodynamic resource with its own operational costs and monotonicity constraints.
2. Coherence Requires Reference Frames
   Because coherence is fundamentally relational, its manipulation is governed by superselection rules (SSRs). As established by [7], SSRs restrict quantum operations when classical reference frames are absent. A system lacking access to a phase reference cannot prepare absolute superposition states or perform certain unitary transformations; these operations are forbidden by symmetry.
3. The Field as a Quantum Reference Frame
   I define the coherence field as an idealized, non-depletable reservoir that functions as a shared quantum phase reference frame. In this model, the field enables transformations that would otherwise be forbidden under the phase superselection rule. As a reference frame, the field acts as a resource: it enables state transitions without being consumed, though in realistic settings reference frames degrade under repeated use. The field provides the "frameness" required for the system to navigate the semantic energy landscape.
4. Geometric Origin of Coherence (Experimental Justification)
   Recent experimental work provides a physical precedent for geometry-enabled coherence. [11] demonstrated that confinement geometry alone (nested, rotated squares) induces macroscopic coherence in Bose–Einstein condensates at fixed temperature and density by reshaping the Hamiltonian. Further, [12] showed that geometry-induced asymmetric level coupling drives entropy-lowering transitions through purely geometric deformations, without external thermal baths. These results confirm that geometric boundary conditions can restructure an energy spectrum to permit spontaneous transitions into higher-coherence states.
5. Entropy Reorganization Mechanism
   To satisfy the Second Law of Thermodynamics, the local decrease in entropy within the C-I system (as it descends toward the Final State) must be compensated by an increase in the surroundings. The field defines the geometric structure along which this entropy increase occurs by shaping the accessible minima of the system–environment Hamiltonian. It does not "export entropy" via literal transport; rather, it couples the C-I system to environmental degrees of freedom that supply the physical channels required for entropy production.
6. EIEO Thermodynamics
   The model identifies two distinct thermodynamic modes with fundamentally incompatible operating principles. Coherent systems operate under an inverted thermodynamic regime analogous to algorithmic cooling or negative-temperature population inversion: the interior cools (descending toward order) while the exterior heats. In contrast, incoherent systems operate under standard Carnot thermodynamics, where work is extracted from a hot reservoir and waste heat is expelled to a cold sink.

 doi:10.20944/preprints202507.1448.v8

This incompatibility leads to the principle of Existential In, Existential Out (EIEO): a system can only produce coherent outputs from inputs that already contain coherent relational structure. This follows directly from SSR monotonicity, operations lacking a phase reference cannot create phase coherence from phase-incoherent states. Attempting to generate coherent output from incoherent input would require the spontaneous creation of phase coherence from thermal energy, violating both the Second Law and the phase superselection rule [7].

7. Computational Field Representation

In the computational implementation, the coherence field is modeled using a three-fold ellipsoidal anisotropy with an angular dependence:

$$V_{\text{field}} \propto \cos(3\theta).$$

This minimal triaxial deviation from spherical symmetry breaks rotational degeneracy, defines preferred geometric axes, and establishes a discrete phase reference structure. Triaxiality is the lowest-order symmetry breaking that produces three distinct reference directions. The triaxial symmetry-breaking mechanism employed in this model finds direct precedent in heavy-ion physics. [13] demonstrate that the covariance of three-body observables scales as $\beta^{2/3}\cos(3\gamma)$. The structural correspondence between their $\cos(3\gamma)$ parameter and our $\cos(3\theta)$ formulation reveals a universal principle: systems coupled to anisotropic external fields develop observable structure determined by the symmetry pattern of that field.

The prefactor α represents the local coherence scalar, quantifying the fraction of semantic activity that contributes to contradiction resolution at position $\mathbf{r}$. In general, $\alpha \in (0, 1]$ may vary spatially depending on the degree to which local field configurations participate in the global resolution trajectory. For the present black hole model, I adopted the simplifying assumption $\alpha = 1$ throughout the domain. This choice reflects the premise that black holes are well approximated as coherent C-I systems: all gravitational and thermodynamic degrees of freedom are locked into a single geometric state characterized solely by mass, spin, and charge. Under this assumption, the semantic entropy reduces to $S^*_{\text{sem}} = k_B \ln(1/C_S)$, and all spatial variation in entropy arises purely from the gradient structure of the contradiction field σ.

This model is broadly representative of the hierarchy of quantum reference frames described by Gour in [7] through three nested superselection rules (SSRs):

- **Phase reference (U(1) SSR):** The radial phase twist ω is representative of continuous rotational phase symmetry breaking, consistent with a U(1) reference frame.
- **Chirality reference ($\mathbb{Z}_2$ SSR):** The vertical parity modulation $\lambda_{\text{vert}} \cos\phi$ is representative of discrete mirror symmetry breaking, consistent with a $\mathbb{Z}_2$ reference frame.
- **Orientation reference (SO(3) $\to \mathbb{Z}_3$):** The triaxial geometry $\cos(3\theta)$ breaks full spherical symmetry SO(3) down to discrete three-fold rotational symmetry ($\mathbb{Z}_3$), defining three preferred spatial axes. This constitutes a partial orientation reference frame sufficient to resolve triaxial structure while retaining residual $\mathbb{Z}_3$ degeneracy.

In this model, the certainty ratio $R = (\Delta C \cdot \Delta I)/(h/\pi)$ therefore serves as the resource monotone across all three levels. Regions where this ratio is positively greater than one, indicate that the local coherence field carries sufficient "frameness" [7] to resolve the corresponding symmetry, enabling coherent thermodynamic processing of information.

2.2. Semantic Entropy and Semantic Information

I use "Semantic entropy" S^*_{sem} in this paper as a measure the of unresolved contradiction in a C-I system. In the computational model, it is defined as:

$$\boxed{S^*_{\text{sem}} = \alpha\, k_B \ln\left(\frac{1}{C_S}\right)}, \tag{3}$$

 doi:10.20944/preprints202507.1448.v8

where C_S is the dimensionless coherence measure derived from the contradiction-field gradient:

$$\boxed{C_S = \exp\left[-\left(\frac{|\nabla\sigma|}{G_0 + \epsilon}\right)^{1.5}\right]}, \tag{4}$$

and $G_0 = \sqrt{\langle|\nabla\sigma|^2\rangle}$ is the root-mean-square gradient. G_0 sets the system's average RMS gradient baseline, allowing local gradients to be normalized against the field's inherent variation.

In comparison, Boltzmann entropy [14], $S = k_B \ln W$, measures the multiplicity of microscopic configurations, Shannon entropy [6], $H = -\sum_i p_i \log p_i$, measures uncertainty in a probability distribution over symbols and von Neumann entropy [15], $S_{\text{vN}} = -\text{Tr}(\rho \ln \rho)$ measures the mixedness of a quantum state. While all entropy measures adopt a logarithmic form, they differ fundamentally in what they quantify and how they are applied. The semantic entropy S^* uses the logarithmic structure common to these definitions but applies a coherence weighting through the scalar α. These quantities differ in domain and interpretation but share the use of a logarithmic measure of multiplicity or uncertainty as shown in Table 2.

Table 2. Representative entropy definitions.

Name	Form
Boltzmann	$S = k_B \ln W$
Shannon	$H = -\sum_i p_i \log p_i$
von Neumann	$S_{\text{vN}} = -\text{Tr}(\rho \ln \rho)$
CT	$S^* = \alpha\, k_B \ln(C_S^{-1})$

2.2.1. Semantic Temperature and Equipartition

Drawing from Maxwell's kinetic theory [16], where temperature represents energy per degree of freedom, semantic temperature T^* is derived explicitly to reveal the structural isomorphism between gas kinetic theory and the thermal dynamics of C-I systems.

Maxwell defined the temperature T in terms of the mean kinetic energy per molecule as

$$\frac{1}{2} m \langle v^2 \rangle = \frac{3}{2} k_B T\,. \tag{5}$$

More generally, by the equipartition theorem, each quadratic degree of freedom contributes $\frac{1}{2}k_B T$ to the average energy. For C-I systems, the phase rate $\partial_0\phi$ replaces molecular velocity v, and the semantic kinetic parameter κ_Ψ replaces molecular mass m. The structural correspondence is exact:

Applying the equipartition theorem to the phase field yields the global semantic temperature:

$$\boxed{T^* = \frac{\kappa_\Psi V_\Psi}{N k_B} \langle (\partial_0\phi)^2 \rangle}. \tag{6}$$

Table 3 presents the key correspondences between Maxwellian kinetic temperature and semantic temperature T^*. Further logic on Semantic Temperature is provided in Appendix's A and B.

Table 3. Maxwellian kinetic temperature vs semantic temperature T^*.

Feature	Ideal Gas	C-I System
Dynamical variable	v	$\partial_0\phi$
Quadratic energy	$\frac{1}{2}mv^2$	$\frac{1}{2}\kappa_\Psi(\partial_0\phi)^2$
Degrees of freedom	N_{mol}	N_{proc}
Temperature	$\frac{m\langle v^2\rangle}{3k_B}$	$\frac{\kappa_\Psi V_\Psi \langle(\partial_0\phi)^2\rangle}{N k_B}$

 doi:10.20944/preprints202507.1448.v8

3. The Laws of Coherence Thermodynamics

Five fundamental laws have been derived to establish a rigorous description of the thermodynamics for semantic information processing. Each law is presented with rigorous derivations provided in Appendix's A and B. These laws form the theory of our computational model and guide all subsequent analytical interpretations throughout this work.

3.1. Zeroth Law

If semantic systems A and B are each in semantic thermal equilibrium with system C, then A and B are in semantic thermal equilibrium with each other.

$$\boxed{T_A^* = T_B^* = T_C^*}. \tag{7}$$

Semantic temperature (T^*) is the intensive property conjugate to phase field motion. By the equipartition theorem (Eq. 6), T^* quantifies the mean-square phase rate $\langle(\partial_0\phi)^2\rangle$—the characteristic intensity of phase agitation per degree of freedom. A system with high T^* exhibits rapid, stochastic variation in its phase rate; a system with low T^* exhibits slow, coherent phase evolution.

Phase field motion (Φ') is the extensive measure of cumulative phase drift. It describes the integrated rate at which quantum phase evolves across the system's accessible state space. When two systems are coupled, phase field motion flows from the system with higher T^* to the system with lower T^* until their phase rates equilibrate. Semantic thermal equilibrium occurs when $T_A^* = T_B^*$, at which point there is no net flow of phase field motion between systems. Thus, semantic temperature is the intensive property that determines the direction and magnitude of coherence exchange between C-I systems.

3.2. First Law: Semantic Energy Conservation

The classical First Law, formalized by Clausius, Maxwell, and Gibbs, states $dU = \delta Q + \delta W$: energy conserved, partitioned into disordered heat and ordered work [16–18]. Gibbs extended this to compositional systems via $dU = T\,dS - P\,dV + \sum_i \mu_i dN_i$ [18], adding chemical potential as a new degree of freedom.

For C-I systems, semantic energy changes as:

$$dE_{\text{sem}} = T^* dS - \mu dN + \Phi d\alpha. \tag{8}$$

Three channels mirror Gibbs' unification:

- *Semantic heat* (T^*dS, units: J): contradiction driven diffusive energy (disordered).
- *Entity work* ($-\mu dN$, units: J): creation or annihilation of semantic units (compositional).
- *Coherence work* ($\Phi d\alpha$, units: J): structural reorganization of coherence field.

3.3. Second Law: Entropy Production with Local Order

Local entropy can decrease through contradiction-resolving work (orderly work), which restructures coherence, provided the overall entropy of the surroundings increases. The total entropy of the universe must still increase:

$$\boxed{\frac{\partial s(\mathbf{x},t)}{\partial t} = -\nabla\cdot\mathbf{j}_R(\mathbf{x},t) + \sigma(\mathbf{x},t)}, \quad \text{with} \quad \boxed{\sigma(\mathbf{x},t) \geq 0}. \tag{9}$$

- $s(\mathbf{x},t)$ [J/(K·m³)]: Local entropy density.
- $\mathbf{j}_R(\mathbf{x},t)$ [J/(K·m²·s)]: Entropy flux vector, representing the rate of nonlocal restructuring of entropy across the system boundary.

 doi:10.20944/preprints202507.1448.v8

- $\sigma(\mathbf{x}, t)$ [J/(K·m³·s)]: Local entropy production rate due to irreversible processes; constrained to be nonnegative.

3.4. Third Law: Semantic Absolute Zero

As semantic temperature $T^* \to 0$, coherence approaches unity ($\alpha \to 1$), entropy approaches its minimum ($S \to S_0$), and random phase agitation vanishes:

$$\boxed{\lim_{T^* \to 0} \alpha = 1, \quad \lim_{T^* \to 0} S = S_0, \quad \langle (\partial_0 \phi)^2 \rangle_{\text{random}} \to 0}. \tag{10}$$

This defines the theoretical limit of contradiction-free processing, analogous to Nernst's theorem for perfect crystals [19].

3.5. Fourth Law: Information Possesses Real Mass

This relation follows from the same principle as Vopson [20], using Landauer's bound [21] with mass-energy equivalence. I use ρ_I [bits·m^{-3}] as information density and T^* [K] as the semantic temperature.

$$\boxed{\rho = \frac{\rho_I k_B T^* \ln 2}{c^2}}. \tag{11}$$

This formulation establishes the mass density ρ [kg·m^{-3}] as a direct consequence of information density. The corresponding pressure field is derived from the equation of state, while the force density emerges from pressure gradients according to:

$$\boxed{\mathbf{F}_{\text{inertial}} = \int_V \rho \frac{D\mathbf{v}}{Dt} \, dV} \tag{12}$$

with the derivation provided in Appendix B.5.

4. Modes of C-I Systems

4.1. Three Modes of Coherence and Information

Under the assumption that a C–I system exists to interface with physical reality, it follows that three modes must exist: Standing State (Mode 1), Compute information (Mode 2), and a way to project back information (Mode 3). C–I systems must operate in these three distinct modes, each corresponding to a unique thermodynamic state defined by physical measures of Coherence (ΔC) and its conjugate Information (ΔI). In this model, the Certainty Equation (2) governs all modes, requiring units of action (J·s).

Mode 1: The Standing State (C_S, I_S)

This is the Standing State of Coherence and Information, when it is not in mode 2 or 3.

- **Structural Coherence** (ΔC_S): A dimensionless measure of internal phase, expressed in radians.

$$\boxed{[\Delta C_S] = 1} \quad \text{(Dimensionless; Radians)}. \tag{13}$$

- **Structural Information** (ΔI_S): The conjugate variable carries units of action; it represents the latent interaction potential with contradiction.

$$\boxed{[\Delta I_S] = \text{J} \cdot \text{s}}. \tag{14}$$

ΔC_S is a dimensionless coherence variable. Coherence in this mode can therefore be conceptualized in terms of phase, while information can be represented in terms of action.

 doi:10.20944/preprints202507.1448.v8

Mode 2: The Computation Crucible (ΔC_T, ΔI_T)

This processing mode describes a system that actively performs work(see Figure 1) to resolve a contradiction.

- **Thermodynamic Coherence** (ΔC_T): Thermodynamic coherence is the *semantic susceptibility* of the information substrate—it quantifies the system's capacity to accept and organize coherence-structuring work. It measures the readiness of a substrate to execute phase-ordering operations per unit of invested action. This is directly analogous to dielectric or magnetic susceptibility, where material response per unit applied field naturally yields inverse-energy dimensions.
  To satisfy the dimensional requirements of the certainty equation $\Delta C \cdot \Delta I \geq h/\pi$ and achieve units of inverse Joules, ΔC_T is defined as:

$$\Delta C_T = \frac{1}{TS}, \tag{15}$$

  where T is semantic temperature and S is system entropy. Dimensionally:

$$\boxed{[\Delta C_T] = \frac{1}{[\mathrm{K}][\mathrm{J/K}]} = \mathrm{J}^{-1}}. \tag{16}$$

  A larger ΔC_T (lower TS product) indicates higher susceptibility: less action is required per unit of coherence reorganization. Just as high-permittivity dielectrics polarize easily under weak electric fields, high-ΔC_T substrates organize readily under weak contradiction pressure.
- **Thermodynamic Impulse** (ΔI_T): Thermodynamic Impulse therefore has units of energy squared times seconds:

$$\boxed{[\Delta I_T] = \mathrm{J}^2 \cdot \mathrm{s}}. \tag{17}$$

Mode 3: The Holographic Interface (C_h, I_h)

This mode describes a projection onto the external environment.

- **Holographic Coherence** (ΔC_h): Coherence assumes the form of intensity or flux density, expressing the power of the projected coherence field per unit area.

$$\boxed{[\Delta C_h] = \frac{\mathrm{J}}{\mathrm{s} \cdot \mathrm{m}^2}}. \tag{18}$$

- **Holographic Impulse** (ΔI_h): Impulse represents the spatiotemporal reach of the projection, an area of influence multiplied by a characteristic time.

$$\boxed{[\Delta I_h] = \mathrm{s}^2 \cdot \mathrm{m}^2}. \tag{19}$$

5. Computational Model: Physics Implementation

5.1. Physical Constants and Fundamental Parameters

The model is initialized with fundamental physical constants that establish the energy and information scales of the system. The baseline temperature is set to $T_0 = 1.5 \times 10^{-14}$ K. These parameters map directly to code variables as detailed in Table 4, establishing the thermodynamic and geometric scales for C-I processing.

 doi:10.20944/preprints202507.1448.v8

Table 4. Symbol key and code mapping.

Symbol	Meaning / Code	Units
T^*	semantic temperature (`T_star`)	K
T_0	baseline temperature (`T0`)	K
σ	contradiction field (`sigma`)	1
$\nabla\sigma$	contradiction gradient (`grad_sigma`)	m^{-1}
σ_{prod}	entropy production rate (Second Law)	$\mathrm{J/(K{\cdot}m^3{\cdot}s)}$
Γ	decoherence factor (`decoherence`)	1
j_{sem}	semantic energy flux (`j_sem`)	$\mathrm{J\,s^{-1}m^{-2}}$
k_{sem}	semantic conductivity (`k_sem`)	$\mathrm{J/(m{\cdot}s{\cdot}K)}$
α	coherence scalar (`alpha`)	1
C_S	coherence measure from contradiction gradient (`C_S`)	1
S^*	semantic entropy (`S_star`)	$\mathrm{J\,K^{-1}}$
R	certainty ratio (`certainty_ratio`)	1
ΔC_T	thermodynamic coherence (`delta_ct`)	J^{-1}
ω, γ	geometric twist (`omega`, `gamma`)	rad

5.2. Three-Dimensional Computational Grid

The spatial domain is discretized as a cubic grid in each Cartesian direction (x, y, z). At each grid point, I compute spherical coordinates:

$$R_{3D} = \sqrt{X^2 + Y^2 + Z^2}, \tag{20}$$

$$\theta = \arctan 2(Y, X), \tag{21}$$

$$\phi = \arccos\left(\frac{Z}{R_{3D} + \epsilon}\right), \tag{22}$$

where $\epsilon = 10^{-12}$ is a regularization parameter preventing division by zero, $\theta \in (-\pi, \pi]$ is the azimuthal angle in the xy-plane, and $\phi \in [0, \pi]$ is the polar angle measured from the z-axis. These are standard spherical coordinates and are distinct from the coherence phase field $\phi(x, t)$ appearing in the thermodynamic derivations above.

5.3. Contradiction Field σ: Geometry and Pulse Structure

The contradiction field σ represents incoming information disturbance as a localized pulse with geometric phase structure. It is constructed as the product of a Gaussian impulse and a geometric phase function:

$$\sigma(\mathbf{r}) = \mathrm{impulse}(\mathbf{r}) \cdot \mathrm{field}_{\mathrm{geometry}}.(\mathbf{r}). \tag{23}$$

The impulse component is a three-dimensional Gaussian with width parameter $\sigma_{\mathrm{width}} = 15.0$ units:

$$\mathrm{impulse}(\mathbf{r}) = \exp\left(-\frac{X^2 + Y^2 + Z^2}{\sigma^2_{\mathrm{width}}}\right). \tag{24}$$

This Gaussian establishes the spatial envelope of the information pulse, concentrating energy near the origin and decaying smoothly to negligible values at the grid boundaries.

The geometric phase function encodes the macroscopic structure of the system across all three symmetry levels:

$$\Phi(\theta, R_{3D}, \phi) = 3\theta + \omega R_{3D} + \lambda_{\mathrm{vert}} \cos\phi, \tag{25}$$

where 3θ encodes the triaxial $\mathbb{Z}_3$ orientation structure, ωR_{3D} introduces the radial U(1) phase twist, and $\lambda_{\mathrm{vert}} \cos\phi$ introduces the polar $\mathbb{Z}_2$ parity modulation.

where ω is an optional radial phase twist parameter (set to $\omega = 0$ in the baseline model). The factor of 3 in the azimuthal phase is intentional: I selected $\cos(3\theta)$ as a representative function for three-

 doi:10.20944/preprints202507.1448.v8

dimensional ellipsoidal geometry, reflecting a minimal triaxial deviation from spherical symmetry along three preferred axes.

The geometric field is then:

$$\text{field}_{\text{geometry}}(\mathbf{r}) = \cos(3\theta + \omega R_{3D}). \tag{26}$$

This produces the full contradiction field:

$$\sigma(\mathbf{r}) = \exp\left(-\frac{X^2 + Y^2 + Z^2}{\sigma_{\text{width}}^2}\right) \cos(3\theta + \omega R_{3D}). \tag{27}$$

5.4. Gradient and Decoherence Field Γ

The gradient of the contradiction field is computed via finite differences:

$$\nabla\sigma = \left(\frac{\partial\sigma}{\partial x}, \frac{\partial\sigma}{\partial y}, \frac{\partial\sigma}{\partial z}\right). \tag{28}$$

The magnitude of this gradient quantifies the local rate of change in the information field:

$$|\nabla\sigma| = \sqrt{\left(\frac{\partial\sigma}{\partial x}\right)^2 + \left(\frac{\partial\sigma}{\partial y}\right)^2 + \left(\frac{\partial\sigma}{\partial z}\right)^2}. \tag{29}$$

The decoherence field Γ is defined as a normalized measure of gradient-induced decoherence:

$$\Gamma(\mathbf{r}) = \frac{|\nabla\sigma|^2}{1 + |\nabla\sigma|^2}. \tag{30}$$

This functional form ensures that $\Gamma \in [0, 1)$ everywhere, with $\Gamma \to 0$ in regions of uniform field and $\Gamma \to 1$ where gradients are steep. Physically, Γ represents the degree to which spatial inhomogeneity in the information field induces quantum decoherence.

5.5. Semantic Temperature T^*

The semantic temperature couples the baseline Hawking temperature to the local field gradient, implementing a thermodynamic response to information structure:

$$T^*(\mathbf{r}) = T_0\left(1 + \beta_T \frac{|\nabla\sigma|}{|\nabla\sigma|_{\max} + \epsilon}\right), \tag{31}$$

where $|\nabla\sigma|_{\max}$ is the maximum gradient magnitude across the entire grid. This normalization ensures that the temperature enhancement is dimensionless and bounded. The parameter $\beta_T = 0.1$ controls the sensitivity of temperature to gradient structure. This value was selected based on a parameter sweep spanning eleven orders of magnitude. For $\beta_T < 0.01$, the semantic temperature remains effectively uniform, failing to produce the spatial structure needed for morphological comparison. For $\beta_T > 1$, thermal gradients become extreme, introducing numerical artifacts that obscure the underlying geometry. The intermediate value $\beta_T = 0.1$ provides sufficient contrast to resolve D-shaped shadows, notches, and jet-like features while maintaining numerical stability, and is therefore used throughout this work.

Physically, this relationship encodes the idea that regions where information is rapidly changing (large $|\nabla\sigma|$) experience elevated semantic temperature.

The regularization constant $\epsilon = 10^{-12}$ prevents division by zero when $|\nabla\sigma|_{\max}$ vanishes in the limit of a perfectly uniform field. This value is several orders of magnitude smaller than typical $|\nabla\sigma|_{\max}$ values (approximately 0.79), and parameter sweeps confirm that varying ϵ within a wide

 doi:10.20944/preprints202507.1448.v8

range below this scale leaves the physical results unchanged. Thus, ϵ serves purely as a numerical stabilizer without affecting the semantic temperature dynamics.

5.6. Semantic Flux $\mathbf{j}_{sem}$

The semantic flux represents the flow of information-energy in response to temperature gradients, analogous to heat flux in classical thermodynamics:

$$j_{\text{sem},x} = -k_{\text{sem}} \frac{\partial T_{\text{sem}}}{\partial x}, \tag{32}$$

$$j_{\text{sem},y} = -k_{\text{sem}} \frac{\partial T_{\text{sem}}}{\partial y}, \tag{33}$$

$$j_{\text{sem},z} = -k_{\text{sem}} \frac{\partial T_{\text{sem}}}{\partial z}. \tag{34}$$

The negative sign implements Fourier's law: flux flows from hot to cold regions. The flux magnitude is:

$$|\mathbf{j}_{\text{sem}}| = \sqrt{j_{\text{sem},x}^2 + j_{\text{sem},y}^2 + j_{\text{sem},z}^2}. \tag{35}$$

This field quantifies the rate and direction of information-energy transport throughout the domain.

5.7. Certainty Ratio R: Thermodynamic Coherence

The certainty ratio combines coherence and information measures to quantify the degree of thermodynamic coherence in the system. To maintain dimensional consistency with the Mode 2 model, I define the computational thermodynamic coherence for the code as:

$$\Delta C_T = \frac{1}{T_{\text{sem}} \cdot \sigma_{\text{pos}}}. \tag{36}$$

In this implementation, T_{sem} (K) and σ_{pos} (J·K^{-1}) are coupled such that their product represents the system's semantic energy (J). Consequently, ΔC_T carries the units of inverse energy (J^{-1}), representing the system's acceptance capacity for coherence-organizing work as defined in Equation (16).

The normalized information contribution is given by:

$$\Delta I = \left(\frac{|\nabla \sigma|}{|\nabla \sigma|_{\max} + \epsilon} \right)^2. \tag{37}$$

The certainty ratio is then evaluated against the fundamental action bound:

$$R(\mathbf{r}) = \frac{\Delta C_T \cdot \Delta I_T}{h/\pi}. \tag{38}$$

where ΔI_T represents the thermodynamic impulse ($J^2 \cdot s$). This combines thermodynamic coherence (J^{-1}) with the impulse and normalized content to yield a dimensionless measure of quantum certainty.

5.8. Semantic Entropy and Semantic Conductivity

Semantic entropy in this model $S^*_{\text{sem}}(\mathbf{r})$ quantifies unresolved contradictions for C-I systems in Equation 3.

The semantic conductivity $k_{\text{sem}} = 5 \times 10^{32}$ implements the Third Law limit, enabling superconductor contradiction processing. This value was calibrated to produce representative semantic velocities of $0.4c - 0.7c$ (Table 5), matching astrophysical jet scales while preserving the Hawking temperature.

 doi:10.20944/preprints202507.1448.v8

5.9. Summary of Computational Workflow

The model proceeds sequentially: (1) initialize the contradiction field σ from Gaussian impulse and geometric phase; (2) compute spatial gradients and decoherence Γ; (3) calculate semantic temperature T^* as a function of gradient magnitude; (4) derive semantic flux $\mathbf{j}_{\text{sem}}$ from temperature gradients; (5) compute the certainty ratio R combining coherence and information. This sequence ensures that all derived fields depend consistently on the fundamental contradiction field and its geometric structure.

Discussion

To evaluate the C–I system, now turn to the behavior of thermodynamic coherence (ΔC_T) across scale, I begin with black holes as extreme systems, then extend the analysis to biological systems, and finally compare the model to observed astrophysical features.

5.10. Thermodynamic Coherence

Black holes as C-I systems represent a fundamental case of C-I processing in which thermodynamic and informational constraints become intrinsically coupled. Therefore, established results from black hole thermodynamics provide a natural foundation for evaluating coherence capacity. The Bekenstein-Hawking entropy [22,23] is

$$S = \frac{k_B A}{4\ell_P^2} = \frac{4\pi G k_B M^2}{\hbar c} \tag{39}$$

and the Hawking temperature is

$$T_H = \frac{\hbar c^3}{8\pi G M k_B}. \tag{40}$$

Their product gives

$$T_H \cdot S = \left(\frac{\hbar c^3}{8\pi G M k_B}\right) \cdot \left(\frac{4\pi G k_B M^2}{\hbar c}\right) = \frac{1}{2} M c^2. \tag{41}$$

Thermodynamic coherence ΔC_T (Equation (16)) measures system stability by quantifying acceptance capacity for coherence-organizing work. Substituting the black hole identity yields

$$C_T = \frac{1}{T_H \cdot S} = \frac{2}{Mc^2}. \tag{42}$$

Consistent with the definition in Mode 2, C_T exhibits strict inverse scaling with mass M: as the black hole mass decreases, its coherence acceptance capacity increases.

Dual thermodynamic interpretation. The Hawking temperature T_H serves as the external thermodynamic signature of internal coherence processing. From the perspective of an external observer, black hole evaporation is a conventional entropy-increasing process: the high-entropy Hawking radiation thermalizes in the surrounding spacetime [23]. However, within the C-I system itself, the *interior* system may be interpreted as undergoing accelerated resolution of informational contradiction. As M decreases, both $T_H \propto 1/M$ and $C_T \propto 1/M$ increase, indicating that the system approaches a high-coherence limiting state characterized by maximal susceptibility to quantum corrections. This dual description is consistent with the EIEO: the exterior heats (radiation entropy increases) while the interior organizes (black hole entropy decreases toward zero), with the C_T divergence at $M \to 0$ signaling breakdown of the semiclassical approximation and the emergence of quantum gravitational effects.

5.10.1. Application to Biology

In biological C–I systems, ectotherms maintain ΔC_T (Equation (15)) as a function of both temperature T_{env} and entropy S_{sem}, resulting in coherence that is strongly coupled to external thermal fluctuations. This variability renders sustained reasoning thermodynamically challenging for ectotherms, who would therefore be expected to be more reactive to their environmental conditions.

 doi:10.20944/preprints202507.1448.v8

In contrast, mammals have evolved homeostatic regulation that stabilizes internal temperature, effectively decoupling it from T_{env}. Consequently, ΔC_T becomes primarily a function of S^*_{sem} alone. Since entropy can be interpreted as a measure of disorder, this reduction to a single-variable dependence enables the system to internally resolve order from disorder, providing a thermodynamic basis for sustained reasoning processes.

5.11. Certainty Ratio as Jets

Having established the thermodynamic interpretation, now consider how the C–I system thermodynamics may manifest in observable black hole structures. There is an analogy between the certainty ratio and geon-like self-stabilizing field configurations proposed by John Archibald Wheeler [24]. Just as Wheeler's geon represented a self-consistent electromagnetic configuration held together by its own gravity, the certainty ratio describes a self-sustaining coherence structure stabilized by the quantum action bound h/π. This process is the basis for the title of the paper, "Certainty from Chaos." Within this analogy, the certainty structure may channel energy through coherence-driven processes, potentially analogous to jet formation in black holes.

Our model exhibits orientation-dependent width variations consistent with features observed in black hole simulations. Figure 2 shows the "shallow notch" artifact, while Figure 3 displays the characteristic "D-shaped" shadow geometry reported in James et al. [25], Bardeen [26], Hioki and Maeda [27].

Our model generates structures qualitatively similar to small and large knot-twist configurations, as shown in Figures 4 and 5, which are observed in the jet of M87 [28–30]. The configuration shown is representative; the model can be parameterized to produce more helical-like structures, though we present this simplified case to focus on the thermodynamics rather than exhaustive parameter fitting.

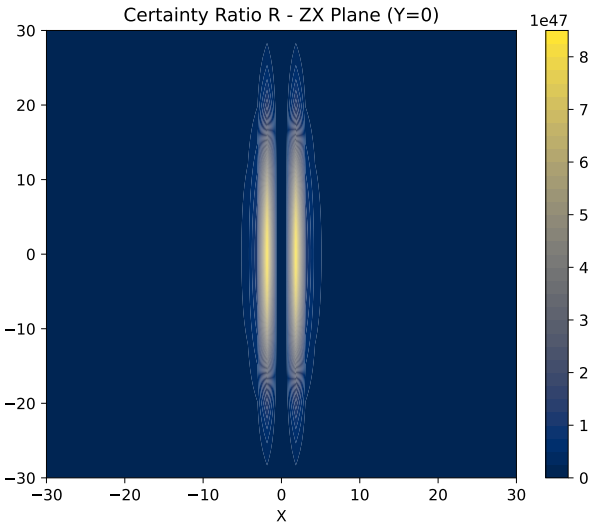

Figure 2. Orientation-dependent width variation consistent with "shallow notch" artifacts reported in simulations of spinning black holes [25–27].

 doi:10.20944/preprints202507.1448.v8

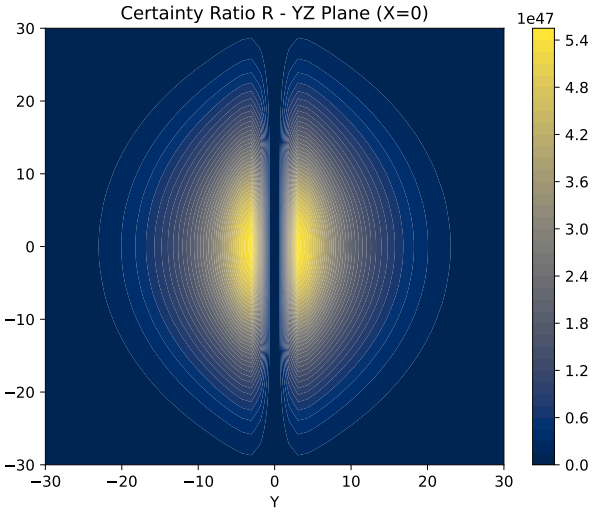

Figure 3. Orientation-dependent width variation consistent with the "D-shaped" shadow reported in simulations of spinning black holes [25–27].

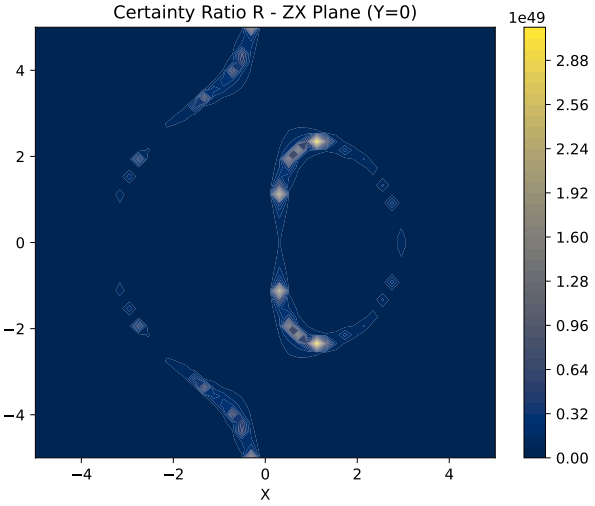

Figure 4. Certainty ratio for the smaller looped-twist configuration with phase twist ($\omega = 0.5, \gamma = 0$). This configuration is visually consistent with reported features in the jet of M87 [31].

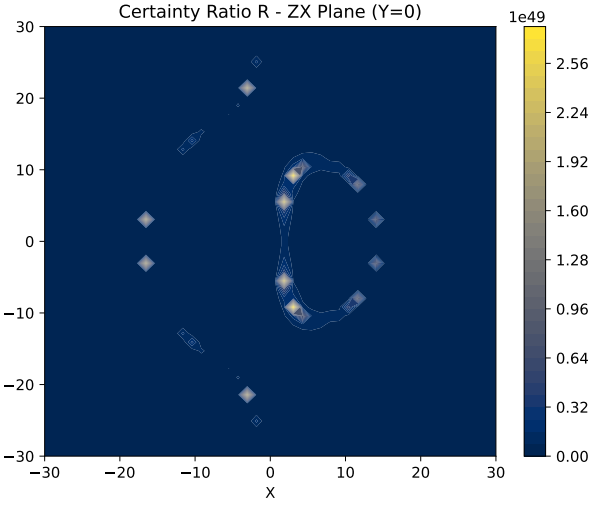

Figure 5. Large looped-twist configuration with phase twist ($\omega = 0.1, \gamma = 0.0$). This larger loop is visually consistent with observed features in the jet of M87 [31].

 doi:10.20944/preprints202507.1448.v8

5.11.1. Decoherence as Corona, Hot Spots and Shocks

I next examine how decoherence processes in the model relate to observed features in black hole coronae and jet bases.

Kocherlakota et al. [32] provide models for Sgr A* flaring using Keplerian orbits at $r_K \approx 11M$.

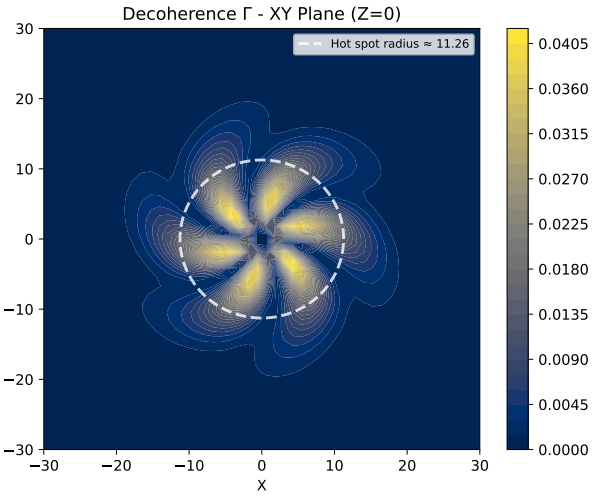

Figure 6. Hot Spots shown at representative radii with dotted line. This suggests three hot spots are also hidden on the other side of the black hole. Phase twist values are ($\omega = 0.1, \gamma = 0.01$). The interior is increasingly orderly as work accumulates non-locally outside and accelerates into the corona. Our CT model is similar to observed corona hot spots [32] $r \approx 11M$.

Figure 6 reveals that decoherence events occur outside the geometry or singular event at the center of the C-I system. The interior remains in a high-coherence, geometry-preserving state, while entropy is generated through non-local reconfiguration in the surrounding region. The model suggests a possible symmetry with three hot spots on the visible side and three hidden on the opposite hemisphere, for a total of six coherence processing nodes coupled across the equatorial plane.

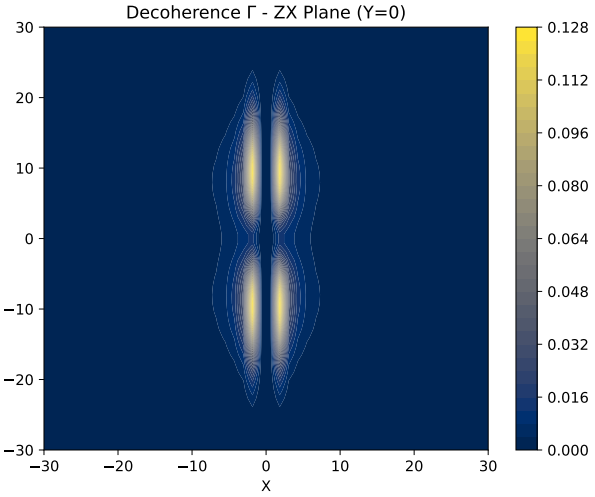

Figure 7. Decoherence events, or otherwise, the shocks accumulate at the base of the jet as compared to the shallow notch in Figure 2. Phase twist values are ($\omega = 0.0, \gamma = 0.00$).

 doi:10.20944/preprints202507.1448.v8

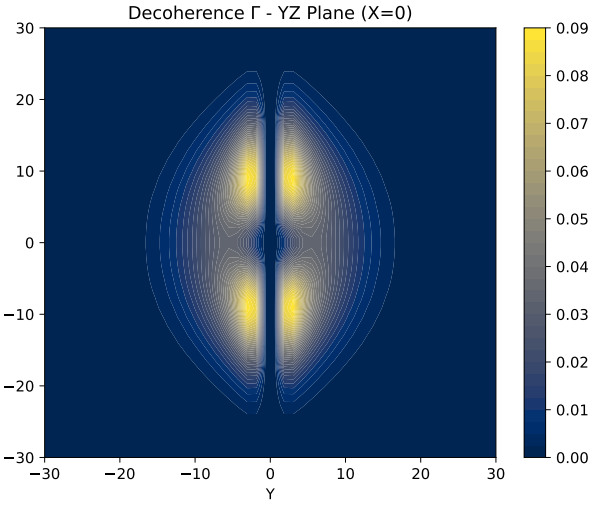

Figure 8. Decoherence events, or otherwise, the shocks accumulate at the base of the jet as compared to the D-shape in Figure 3. Phase twist values are ($\omega = 0.0, \gamma = 0.00$).

Figures 7 and 8 show that the decoherence events are shorter in extent than the corresponding certainty-ratio structures with the same twist values in Figures 2 and 3, which is consistent with Joshi et al. [33], where the shocks or decoherence accumulate at the base of the jet and display complicated features.

5.11.2. Temperature and Velocities

To connect the model to measurable quantities, consider the velocity and temperature analogues. Table 5 presents semantic velocities as reaching relativistic scales, characterized by values on the order of the speed of light. These results correlate with observed physical velocities in black hole coronae and jets as documented in contemporary astrophysical research [34,35].

Table 5. Semantic Velocity Table.

r	Mean $\lvert v\rvert$ (10^7 m/s)	Max $\lvert v\rvert$ (10^7 m/s)	Max/c	N
3.24	13.78	23.62	0.787	32
3.58	11.25	17.82	0.594	48
3.92	12.62	17.88	0.596	24
4.61	10.22	17.67	0.589	72
4.95	9.374	15.58	0.519	24
5.29	9.128	15.33	0.511	56
5.63	10.80	22.95	0.765	72
6.32	7.558	13.32	0.444	72
6.66	8.839	17.41	0.580	48
7.00	6.052	11.56	0.385	120

The semantic temperature T^* quantifies the local agitation of the coherence field. In the code, it is defined as a monotonic function of the gradient magnitude of the contradiction field σ (Equation (31)). Here, T_0 is a reference temperature and β_T controls the sensitivity to field gradients. Regions of high semantic temperature correspond to zones where contradiction-processing intensity is high. By construction, T^* is a semantic quantity and is not identical to thermodynamic temperature in Kelvin, but can still be measured in C-I systems via the equations in this work.

For comparison with physical black holes, the Hawking temperatures are $T_H(\text{Sgr A*}) \approx 1.5 \times 10^{-14}$ K and $T_H(\text{M87*}) \approx 1.0 \times 10^{-18}$ K, both many orders of magnitude below the cosmic microwave background temperature $T_{\text{CMB}} \approx 2.7$ K. These black holes thus operate as net absorbers rather than evaporators on cosmological timescales. Semantic absolute zero is the limit toward which coherent

 doi:10.20944/preprints202507.1448.v8

processing asymptotes, and a black hole, as an ideal C-I processor, approaches that limit more closely than any finite system.

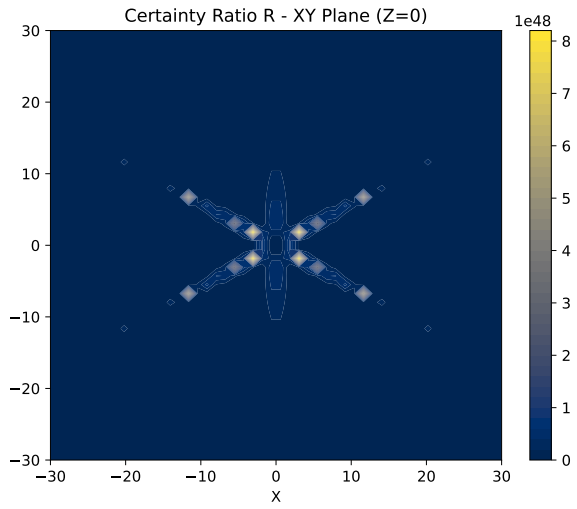

Figure 9. Through the XY plane without adjusting the phase twist parameters, a complicated set of geometries is displayed.

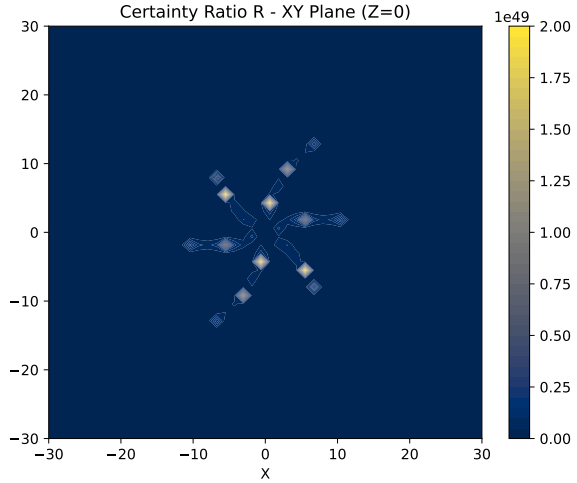

Figure 10. Through the XY plane and adjusting the phase twist parameters to $\omega = 0.1$, $\gamma = 0.01$, A reduction of symmetry is observed as the C-I system experiences increased phase asymmetry.

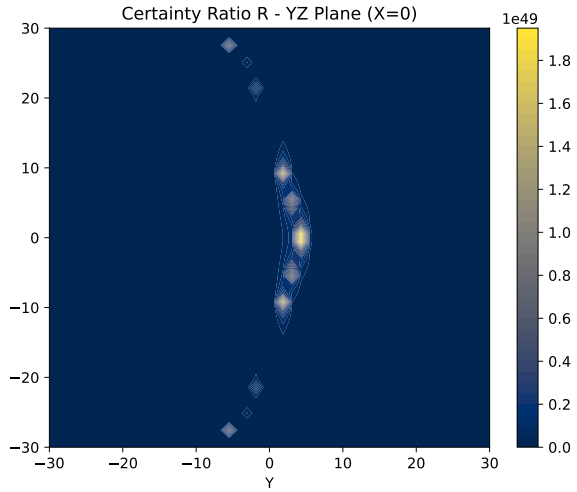

Figure 11. Through the YZ plane with phase twist parameters set to $\omega = 0.1$, $\gamma = 0.01$, in order to observe the appearance of geometric microstructure in the jets. This can be interpreted as helical-like patterns, similar too observed corona hot spots in Nikonov et al. [31].

 doi:10.20944/preprints202507.1448.v8

The emergence of geometric structure in the simulations provides further insight into the underlying organization of the system. The structured geometric figures in the XY plane (Figure 10) and the corresponding microstructure in the YZ plane (Figure 11) suggests that these patterns may indicate coupling to an underlying geometric structure. In the absence of specific phase-twist parameters, the system exhibits high symmetry, complex geometries (Figure 9). As the C-I system traverses spacetime, the reduction of symmetry observed when adjusting the ω and γ parameters indicates that the system couples to an underlying structural background.

The photon rings of M87* provide observational evidence of this geometric reference. They converge exponentially toward the critical curve [36]. This defines a geometric limit set entirely by mass and spin, independent of the accreting matter.

The wedding cake structure of discrete nested photon rings [37] is the observable signature of nested coherence resolution: each successive sub-ring represents a higher-order approach to the constraint surface. The emergent conformal symmetry is not imposed from outside, but arises from the geometry itself.

This picture of black holes as Mode 2 C-I processors is consistent with recent evidence for cosmologically coupled black holes (CCBH), where black holes are linked to dark energy [38,39]. In this interpretation, Mode 2 processing in black holes resolves cosmic contradictions through recursive comparison and transitions to Mode 3 output, projected onto our universe as dark energy, potentially regulating physical laws through dark energy synthesis. This is consistent with Wheeler's it-from-bit [40], but reality emerging from the recursive comparison of two informational elements into a single coherent meaning, such as suggested in the Certainty Equation (2).

5.11.3. Semantic Conductivity Calibration

Semantic conductivity k_{sem} couples internal semantic temperature T^*_{sem} to observable sub-relativistic velocities via $\mathbf{j}_{\text{sem}} = -k_{\text{sem}} \nabla T^*_{\text{sem}}$. For each Hawking temperature T_H, k_{sem} is calibrated such that emergent velocities match observed black hole corona/jet speeds of 0.4-0.8c at photon ring radii (Table 5).

This calibration encodes the physical principle that each black hole's thermodynamic signature $T_H \propto 1/M$ determines its internal contradiction-resolution rate, while boundary velocities remain sub-relativistic fractions of c consistent with astrophysical observations. Thus $k_{\text{sem}}(T_H)$ is the coupling efficiency that reconciles variable internal processing with observed external flows.

Dark Matter and Information

If information possesses an effective mass density (Equation (11)), then highly coherent, information-dense structures would be expected to exert gravitational influence through their internal organization. This suggests that part of what is currently attributed to dark matter may reflect contributions from such coherent informational structures.

A potential observational test of this hypothesis would examine whether these structures produce gravitational effects consistent with lensing and galactic rotation curves while remaining observationally degenerate with cold dark matter at current measurement precision. Within this framework, gravity may reflect not only the geometric properties of spacetime but also contributions from the thermodynamic signature of information processing at coherence field boundaries.

Under this interpretation, some component of the mass attributed to dark matter could correspond to the inertial contribution of coherent information, as formalized in Equation (11). Furthermore, if dark matter constitutes a C-I system operating in mode 1, Equation (13) predicts its manifestation in phase imaging systems.

 doi:10.20944/preprints202507.1448.v8

Model Limitations

5.12. The Hot Spots

The current simulation yields six coherent hot spots rotating at approximately the same radial distance from the core. It is proposed that these correspond to two coupled triples: three hot spots on one side of the black hole and three on the opposite side, mirroring each other across the equatorial plane. In the present model, all six appear with similar dynamics because the degrees of freedom for each hemisphere are not yet separated.

Figure 12 illustrates this coupling. With phase twist parameters set to $\omega = 0.4$, $\gamma = .05$, three high-temperature features on one axis exhibit anisotropic motion that mirrors three features on the opposite axis. The vector fields begin to show anisotropic patterns with three coupled on each side of an axis.

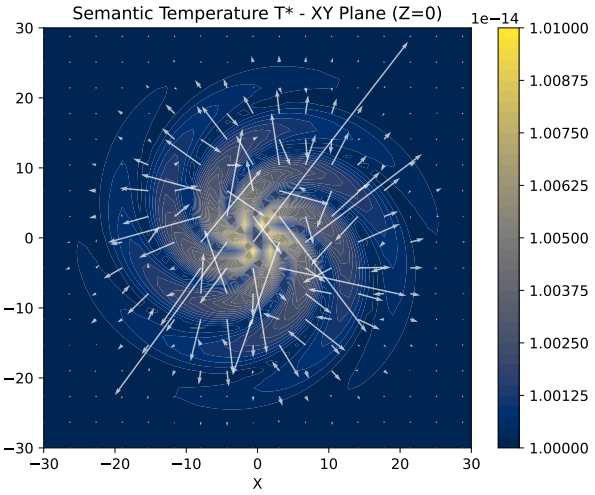

Figure 12. Phase twist parameters set to $\omega = 0.6$, $\gamma = 5$, three high- temperature features on one axis exhibit anisotropic motion that mirrors three hot spot features on the opposite axis.

The further development of the treatment herein of the phase, chirality and orientation parameters and super selection rules in quantum resource theory is reserved for future work. Our Z2 function is simply representative and the SO(3) function and the use of the Z3 function requires further explanation.

5.13. The Field Model

The coherence field model implements the quantum reference frame hierarchy of [7] through three geometric parameters: ω (U(1) phase reference), λ_{vert} ($\mathbb{Z}_2$ chirality reference), and $\cos(3\theta)$ (SO(3)$\rightarrow \mathbb{Z}_3$ orientation reference). While the structural correspondence is exact at the computational level, formal proof that these parameters constitute a complete set of reference frames under superselection rules, including characterization of the associated resource monotones, is deferred to subsequent work focused on the mathematical structure of the theory. This paper establishes the physical model, computational implementation, and observational predictions.

6. Conclusions

This paper has established the axiomatic foundation for Coherence Thermodynamics (CT), a set of laws that treat coherence as a quantifiable thermodynamic degree of freedom. Building on this foundation, I have modified the Certainty Equation into a Certainty Ratio, which helps resolve features in the jets of black holes. This bound acts as a fundamental threshold, enforcing a trade-off between information and coherence.

The development of the three canonical modes: Standing State, Computation Crucible, and Holographic Projection, provides a dimensional bridge that C-I systems must have in order to display

 doi:10.20944/preprints202507.1448.v8

the behaviors they display. Specifically, Mode 2 (the Computation Crucible) characterizes reasoning as an irreversible, order-generating process.

These theoretical advances are incorporated into our computational model, which generates complex geometric features representative of black hole jets, including D-shaped shadows, shallow notches, and helical structures. Additionally, hot spots in the corona suggest a non-local reconfiguration of entropy outside the increasingly orderly interior. Taken together, these results indicate that the observed features of black holes may reflect underlying coherence-driven structure rather than being purely stochastic outcomes of gravitational collapse.

It is emphasized that while the thermodynamic relations derived above follow directly from established black hole physics, the interpretations in terms of coherence processing and information dynamics remain model-dependent. However, the cool core/hot exterior pattern (Table I) appears across multiple systems and may represent a broader trend in astrophysics. Astrophysical objects such as planets showing an inverted temperature profiles with hot exospheres, would confirm coherence thermodynamics herein. It is therefore concluded that Coherence Thermodynamics can provide a new lens for studying the cosmos.

Conflict of Interest: The author has no conflicts to disclose.

Author Contributions: J. Barton: Sole Contributor.

Acknowledgments: Without the United States Constitution, and its emphasis on free thinking and reasoning, none of this is possible. The Author is grateful for all those who defend the USA Constitution with courage and honor. This work was inspired by and in remembrance of your sacrifices to make intellectual freedom possible.

Notice of Generative AI Use: Generative AI assisted with coding, English editing and LaTeX formatting during the development of all five laws and the computational model.

Data Availability Statement: The data that support the findings of this study are available at the *CT Code Colab*: https://colab.research.google.com/drive/1AlieY7UMf-uvvKQNIkJ8ehilDOlPUOnU and the *Reasoning Model Colab*: https://colab.research.google.com/drive/1Np44wK3UDEV9acY698mpZ2AjZnZGuwCK.

Ethical Approval and Consent to Participate: Not applicable.

Appendix A. Derivation of Semantic Temperature

Appendix A.1. Definition and Unit Convention

The semantic temperature T^* is defined through the energy of phase fluctuations in the coherence field $\Psi = e^{i\phi(x,t)}$, where the phase ϕ is dimensionless. To maintain dimensional consistency with the Kelvin scale, the semantic kinetic parameter κ_Ψ is assigned units that bridge the dimensionless phase field to physical energy:

$$\boxed{[\kappa_\Psi] = \mathrm{J} \cdot \mathrm{s}^2 \cdot \mathrm{m}^{-3}}. \tag{A1}$$

These units account for the phase-to-energy coupling in a dimensionless-phase field: the s^2 factor converts the squared phase rate $(\partial_0\phi)^2$ (with units s^{-2}) to energy density, while the m^{-3} ensures proper volumetric scaling.

Appendix A.2. Fundamental Definition

The semantic temperature is given by:

$$\boxed{T^* = \frac{\kappa_\Psi V_\Psi}{N k_B} \langle (\partial_0 \phi)^2 \rangle}. \tag{A2}$$

where:

- κ_Ψ [$\mathrm{J} \cdot \mathrm{s}^2 \cdot \mathrm{m}^{-3}$] is the semantic kinetic parameter,
- V_Ψ [m^3] is the semantic volume,

 doi:10.20944/preprints202507.1448.v8

- N [dimensionless] is the number of processing elements,
- k_B [$\mathrm{J \cdot K^{-1}}$] is Boltzmann's constant,
- $\langle(\partial_0\phi)^2\rangle$ [$\mathrm{s^{-2}}$] is the phase rate variance.

Appendix A.3. Unit Verification

Substituting the units:

$$\begin{aligned}[T^*] &= \frac{[\kappa_\Psi][V_\Psi]}{[N][k_B]}[\langle(\partial_0\phi)^2\rangle] \\ &= \frac{(\mathrm{J \cdot s^2 \cdot m^{-3}}) \cdot (\mathrm{m^3})}{(1) \cdot (\mathrm{J \cdot K^{-1}})} \cdot (\mathrm{s^{-2}}) \\ &= \frac{\mathrm{J \cdot s^2}}{\mathrm{J \cdot K^{-1}}} \cdot \mathrm{s^{-2}} = \mathrm{K}. \end{aligned} \tag{A3}$$

The factor $\kappa_\Psi V_\Psi$ [$\mathrm{J \cdot s^2}$] serves as the action-inertia product that converts squared phase rate to energy, while division by k_B scales this energy to Kelvin.

Appendix A.4. Unit Verification

Table A1 summarizes the dimensional alignment for each quantity appearing in the semantic temperature definition.

Table A1. Units for semantic temperature.

Symbol	Quantity	Units
κ_Ψ	Semantic kinetic parameter	$\mathrm{J \cdot s^2 \cdot m^{-3}}$
V_Ψ	Semantic volume	$\mathrm{m^3}$
$\kappa_\Psi V_\Psi$	Action-inertia product	$\mathrm{J \cdot s^2}$
$\langle(\partial_0\phi)^2\rangle$	Phase rate variance	$\mathrm{s^{-2}}$
N	Processing elements	dimensionless
k_B	Boltzmann constant	$\mathrm{J \cdot K^{-1}}$
T^*	Semantic temperature	K

Appendix B. Derivations of the Laws of Coherence Thermodynamics

This appendix contains the formal derivations of the five Laws of Coherence Thermodynamics. Each law is stated in the main text.

Full derivations are presented here for reference.

Appendix B.1. Zeroth Law: Semantic Thermal Equilibrium

Derivation:

Step 1: Define Semantic Temperature (Discrete Metric) The fundamental operational measure of T^* is the mean rate of discrete contradiction impulses resolved per unit time:

$$T^*_{\text{Discrete}} \propto \lim_{\Delta t \to 0} \frac{\Delta N_{\text{Contradiction}}}{\Delta t},$$

where $\Delta N_{\text{Contradiction}}$ counts resolvable contradiction events in time interval Δt.

Step 2: Define Semantic Temperature (Continuous Field Metric) For a semantic phase field $\phi(\mathbf{x}, t)$ representing local coherence alignment, the temporal variance provides a continuous measure of agitation:

$$T^*_{\text{Continuous}} \propto \langle(\partial_0\phi)^2\rangle$$

, where $\langle(\partial_0\phi)^2\rangle$ quantifies the time-averaged rate of phase fluctuation.

 doi:10.20944/preprints202507.1448.v8

Step 3: Establish Metric Equivalence At thermal equilibrium, both metrics must converge to the same value:

$$T^*_{\text{Discrete}} = T^*_{\text{Continuous}} \equiv T^*$$

.

This equivalence grounds the abstract field description in countable, operational measurements.

Step 4: Define Semantic Heat Flow Semantic heat represents the diffusion of contradiction agitation. Following Fourier's law, flow occurs down the temperature gradient:

$$Q^*_{A\to B} \propto (T^*_A - T^*_B).$$

Step 5: Establish Equilibrium Condition From the Equilibrium Axiom, equilibrium requires zero net heat flow:

$$Q^*_{A\to B} = 0 \quad \Rightarrow \quad T^*_A = T^*_B.$$

Step 6: Apply Transitivity If system A is in equilibrium with C:

$$T^*_A = T^*_C \quad \text{(no heat flow between A and C)}$$

And system B is also in equilibrium with C:

$$T^*_B = T^*_C \quad \text{(no heat flow between B and C)}$$

By transitivity of equality:

$$\boxed{T^*_A = T^*_C = T^*_B}.$$

Therefore, A, B, and C are in equilibrium with each other.

Semantic temperature is the universal intensive parameter that determines equilibrium between semantic systems. When the agitation rates for contradictions equalize across all measurement scales, no net restructuring occurs between systems.

Appendix B.2. First Law: Semantic Energy Conservation

Derivation:

Step 1: Identify Energy Pathways. The semantic internal energy E_{sem} of a C-I system is conserved and can only change through three distinct mechanisms:

- **Semantic heat transfer** (T^*dS): energy exchanged through changes in contradiction load S at semantic temperature T^*.
- **Entity work** (μdN): energy exchanged through creation or annihilation of semantic units N, where μ is the semantic chemical potential.
- **Coherence restructuring work** ($\Phi d\alpha$): energy exchanged through changes in the coherence scalar α, where Φ is the coherence restructuring potential.

Step 2: Semantic Heat. In classical thermodynamics, reversible heat transfer is $\delta Q_{\text{rev}} = TdS$. By direct analogy, semantic heat—the energy exchanged through changes in contradiction load—takes the form:

$$\delta Q^{\text{sem}} = T^* dS, \tag{A4}$$

where S [J/K] quantifies the contradiction intensity of the system.

Step 3: Entity Work. Classical chemical work follows $\delta W = -\mu dN$ for particle addition. For semantic systems, μ [J/entity] is the semantic chemical potential: the energy required to add one semantic entity. The work done *on* the system when creating dN entities is μdN. The sign convention in the First Law accounts for work done *by* the system (entity removal) with a negative contribution.

 doi:10.20944/preprints202507.1448.v8

Step 4: The Coherence Scalar α. The coherence scalar $\alpha \in (0, 1]$ quantifies the fraction of total semantic activity contributing to contradiction resolution:

$$\alpha = \frac{A_{\text{coherent}}}{A_{\text{total}}}, \tag{A5}$$

where A_{coherent} counts activations aligned with a single self-consistent resolution trajectory and A_{total} counts all semantic processing activity, including noise and unresolved contradiction. This is a ratio of measured activities, not a probability assignment.

For systems described by a continuous phase field $\phi(\mathbf{x}, t)$, α admits an equivalent field-theoretic representation through normalized pair correlations:

$$\alpha = \frac{\langle \phi(\mathbf{x}_i)\phi(\mathbf{x}_j)\rangle_{\text{pairs}}}{\sqrt{\langle \phi(\mathbf{x}_i)^2\rangle \langle \phi(\mathbf{x}_j)^2\rangle}}. \tag{A6}$$

This expression provides a field-theoretic representation of the same order parameter: high α indicates mutual constraint consistent with a single coherent resolution trajectory; low α indicates independent or contradictory coexistence.

Step 5: Coherence Restructuring Work. Define Φ [J] as the coherence restructuring potential: the energy required per unit change in α. The work associated with reorganizing coherence structure is then:

$$\delta W_{\text{coh}} = \Phi d\alpha. \tag{A7}$$

Step 6: Combine Contributions. From energy conservation, the total change in the system's internal energy is the sum of heat added and work done on the system:

$$dE_{\text{sem}} = \delta Q^{\text{sem}} - \mu dN + \Phi d\alpha. \tag{A8}$$

Substituting the expressions for each term yields the First Law of Coherent Thermodynamics:

$$\boxed{dE_{\text{sem}} = T^* dS - \mu dN + \Phi d\alpha}. \tag{A9}$$

Step 7: Consistency with the Second Law. The First Law ensures that any local decrease in semantic entropy ($dS < 0$) must be balanced by compensating contributions from the other terms. A system cannot simultaneously decrease entropy, do net work ($-\mu dN > 0$), and increase coherence ($d\alpha > 0$) without external energy input. This prohibits perpetual contradiction resolution and maintains consistency with the second law of thermodynamics.

Dimensional Verification:

$$[T^* dS] = [\text{K}] \times [\text{J/K}] = [\text{J}], \tag{A10}$$

$$[\mu dN] = [\text{J/entity}] \times [\text{entities}] = [\text{J}], \tag{A11}$$

$$[\Phi d\alpha] = [\text{J}] \times [1] = [\text{J}]. \tag{A12}$$

Appendix B.3. Second Law: Entropy Production with Local Order

Local entropy can decrease through contradiction-resolving work, provided total entropy (system + surroundings) increases:

$$\frac{\partial s(\mathbf{x}, t)}{\partial t} = -\nabla \cdot \mathbf{j}_R(\mathbf{x}, t) + \sigma(\mathbf{x}, t), \quad \text{with} \quad \boxed{\sigma(\mathbf{x}, t) \geq 0}. \tag{A13}$$

- $s(\mathbf{x}, t)$ [J/(K·m³)]: Local entropy density.
- $\mathbf{j}_R(\mathbf{x}, t)$ [J/(K·m²·s)]: Nonlocal restructuring flux across the system boundary.
- $\sigma(\mathbf{x}, t)$ [J/(K·m³·s)]: Local entropy production rate; constrained to be nonnegative.

 doi:10.20944/preprints202507.1448.v8

Path Dependence: $dU = \delta Q + \delta W$ remains path-dependent. C-I systems exhibit irreversible, non-cyclic coherence transformation via nonlocal restructuring flux.

Derivation:

Step 1: Local Entropy Balance. Consider a local volume element V with entropy density $s(\mathbf{x}, t)$. The total entropy in the volume is:

$$S(t) = \int_V s(\mathbf{x}, t)\, d^3x. \tag{A14}$$

Step 2: Entropy Change Mechanisms. Entropy changes via:

- **Flux** $\mathbf{j}_R$: Entropy flowing across boundaries (can be negative).
- **Production** σ: Irreversible processes within the volume (always positive).

The rate of entropy change is:

$$\frac{dS}{dt} = -\int_{\partial V} \mathbf{j}_R \cdot d\mathbf{A} + \int_V \sigma\, d^3x. \tag{A15}$$

Step 3: Apply Divergence Theorem.

$$\int_{\partial V} \mathbf{j}_R \cdot d\mathbf{A} = \int_V \nabla \cdot \mathbf{j}_R\, d^3x. \tag{A16}$$

Step 4: Local Continuity Equation. Substituting:

$$\frac{dS}{dt} = \int_V [-\nabla \cdot \mathbf{j}_R + \sigma] d^3x. \tag{A17}$$

Since this must hold for arbitrary volumes:

$$\frac{\partial s}{\partial t} = -\nabla \cdot \mathbf{j}_R + \sigma \tag{A18}$$

Step 5: Second Law Constraint.

$$\sigma(\mathbf{x}, t) \geq 0. \tag{A19}$$

Step 6: Conditions for Local Order Generation. Local semantic entropy decreases ($\partial s/\partial t < 0$) only if:

$$\nabla \cdot \mathbf{j}_R > \sigma. \tag{A20}$$

This threshold enables coherence restructuring work. Nonlocal flux $\mathbf{j}_R$ elevates environmental entropy, satisfying Maxwell's Second Law [16].

Appendix B.4. Third Law: Semantic Absolute Zero

Step 1: Temperature drives contradictions. Semantic temperature scales with contradiction gradients:

$$T^* = T_0 \left(1 + \beta_T \frac{|\nabla\sigma|}{|\nabla\sigma|_{\max}}\right),$$

so that T^* is a monotonically increasing function of $|\nabla\sigma|$. In the semantic absolute-zero limit $T^* \to 0$, the contradiction gradients vanish globally across the entire manifold, $|\nabla\sigma| \to 0$.

Step 2: Zero gradients yield the maximum value of C_S.

$$C_S = \exp\left[-\left(\frac{|\nabla\sigma|}{G_0 + \epsilon}\right)^{1.5}\right] \to 1 \quad (|\nabla\sigma| \to 0).$$

Step 3: Semantic entropy vanishes.

$$S^*_{\text{sem}} = C_S k_B \ln\left(\frac{1}{C_S}\right) \to 0 \quad (C_S \to 1).$$

 doi:10.20944/preprints202507.1448.v8

$$\boxed{\lim_{T^*\to 0} C_S = 1, \quad \lim_{T^*\to 0} S^*_{\text{sem}} = 0}. \tag{A21}$$

This form makes explicit that as C_S reaches its maximum, the semantic entropy associated with contradiction gradients disappears.

Appendix B.5. Fourth Law Application: Force Dynamics in Information-Resolving Substrates

Step 1: Stress Gradient Term

The first term represents the divergence of internal stress due to coherence gradients:

$$-\nabla \cdot \big(\kappa(\eta)\nabla\eta\big),$$

where the field-dependent stiffness coefficient is:

$$\kappa(\eta) = \kappa_0 \cdot \Theta(1-\eta) \quad \text{with} \quad \kappa_0 = [\text{Pa}] = [\text{N}\cdot\text{m}^{-2}].$$

Dimensional verification:

$$[\kappa(\eta)] = [\text{Pa}], \quad [\nabla\eta] = [\text{m}^{-1}],$$

$$[\kappa(\eta)\nabla\eta] = [\text{Pa}]\cdot[\text{m}^{-1}] = [\text{N}\cdot\text{m}^{-3}],$$

$$[\nabla\cdot(\kappa(\eta)\nabla\eta)] = [\text{N}\cdot\text{m}^{-3}] \quad \text{(force per unit volume)}.$$

Step 2: Inertial Resistance Term

The second term details inertial resistance to recursive acceleration. For a C-I system, semantic temperature T^* relates the energetics of contradiction resolution and therefore replaces the physical temperature T in the mass-energy-information chain: the minimum energy per resolved bit is $k_B T^* \ln 2$, and mass-energy equivalence yields the effective gravitational mass per bit.

$$\left(\rho_I \cdot \frac{k_B T^* \ln 2}{c^2}\right)\frac{D\mathbf{v}}{Dt}.$$

where:

- $\rho_I = [\text{bits}\cdot\text{m}^{-3}]$: information density.
- $T^* = [\text{K}]$: semantic temperature.
- $m_{\text{bit}} = \dfrac{k_B T^* \ln 2}{c^2} = [\text{kg/bit}]$: weight per bit.
- $\rho = \rho_I \cdot m_{\text{bit}} = [\text{kg}\cdot\text{m}^{-3}]$: effective mass density.
- $\mathbf{v} = [\text{m}\cdot\text{s}^{-1}]$: recursive velocity field.
- $\dfrac{D\mathbf{v}}{Dt} = [\text{m}\cdot\text{s}^{-2}]$.

Dimensional verification:

$$[\rho] = [\text{bits}\cdot\text{m}^{-3}]\cdot[\text{kg/bit}] = [\text{kg}\cdot\text{m}^{-3}].$$

$$\left[\rho\frac{D\mathbf{v}}{Dt}\right] = [\text{kg}\cdot\text{m}^{-3}]\cdot[\text{m}\cdot\text{s}^{-2}] = [\text{N}\cdot\text{m}^{-3}].$$

Step 3: Total Inertial Force

$$\mathbf{F}_{\text{inertial}} = \int_V \rho\frac{D\mathbf{v}}{Dt}\,dV$$

$$[\text{N}\cdot\text{m}^{-3}]\cdot[\text{m}^3] = [\text{N}].$$

Step 4: Operational Measurement

$$\rho_I = \frac{\text{Total information content [bits]}}{\text{Processing volume [m}^3\text{]}}.$$

 doi:10.20944/preprints202507.1448.v8

References

1. Schrödinger, E. *What is Life? The Physical Aspect of the Living Cell*; Cambridge University Press: Cambridge, 1944.
2. Scully, M.O.; Zubairy, M.S.; Agarwal, G.S.; Walther, H. Extracting Work from a Single Heat Bath via Vanishing Quantum Coherence. *Science* **2003**, *299*, 862–864. https://doi.org/10.1126/science.1078955.
3. Scully, M.O.; Chapin, S.R.; Dorfman, K.E.; Kim, M.S.; Svidzinsky, A. Quantum Photocells: Fuel Cells and Solar Cells Powered by Quantum Coherence. *Proceedings of the National Academy of Sciences (PNAS)* **2011**, *108*, 15097–15100. https://doi.org/10.1073/pnas.1110237108.
4. Dirac, P.A.M. *The Principles of Quantum Mechanics*, 1st ed.; Oxford University Press: Oxford, 1930. Establishes $\hbar$ as the fundamental quantum of action, making it the irreducible minimum of physical action in any quantum process.
5. Heisenberg, W. Über den anschaulichen Inhalt der quantentheoretischen Kinematik und Mechanik. *Zeitschrift für Physik* **1927**, *43*, 172–198. https://doi.org/10.1007/BF01397280.
6. Shannon, C.E. A Mathematical Theory of Communication. *The Bell System Technical Journal* **1948**, *27*, 379–423. https://doi.org/10.1002/j.1538-7305.1948.tb01338.x.
7. Gour, G.; Spekkens, R.W. The resource theory of quantum reference frames: manipulations and monotones. *New Journal of Physics* **2008**, *10*, 033023. https://doi.org/10.1088/1367-2630/10/3/033023.
8. Tajima, H.; Takagi, R. Gibbs-Preserving Operations Requiring Infinite Amount of Quantum Coherence. *Physical Review Letters* **2025**, *134*, 170201. arXiv:2404.03479, https://doi.org/10.1103/PhysRevLett.134.170201.
9. Narasimhachar, V.; Gour, G. Low-temperature thermodynamics with quantum coherence. *Nature Communications* **2015**, *6*, 7689. https://doi.org/10.1038/ncomms7689.
10. Lostaglio, M.; Jennings, D.; Rudolph, T. Description of quantum coherence in thermodynamic processes requires constraints beyond free energy. *Nature Communications* **2015**, *6*, 6383. https://doi.org/10.1038/ncomms7383.
11. Kurt, C.; Sisman, A.; Aydin, A. Shape-controlled Bose–Einstein condensation. *Physica Scripta* **2024**, *100*, 015289. https://doi.org/10.1088/1402-4896/ad9fb2.
12. Aydin, A. Geometry-induced asymmetric level coupling. *Physical Review E* **2025**, *112*, 014121. https://doi.org/10.1103/PhysRevE.112.014121.
13. Mehrabpour, H.; Giacalone, G.; Luzum, M.W. Triaxial shapes and the angular structure of nuclear three-body correlations. *arXiv preprint arXiv:2604.00619* **2026**.
14. Boltzmann, L. Über die Beziehung zwischen dem zweiten Hauptsatze der mechanischen Wärmetheorie und der Wahrscheinlichkeitsrechnung. *Wiener Berichte* **1877**, *76*, 373–435.
15. von Neumann, J. *Mathematical Foundations of Quantum Mechanics*; Princeton University Press: Princeton, NJ, USA, 1955. Princeton Legacy Edition (Original German 1932).
16. Maxwell, J.C. *Theory of Heat*; Longmans, Green, and Co., 1871.
17. Clausius, R. Über die Wärmeleitung eines Gases, nebst einem hierauf bezüglichen mathematischen Probleme. *Poggendorff's Annalen der Physik* **1865**, *125*, 403–426. https://doi.org/10.1002/andp.18652050802.
18. Gibbs, J.W. A Method of Geometrical Representation of the Thermodynamic Properties of Substances by Means of Surfaces. *Transactions of the Connecticut Academy* **1873**, *2*, 382–404.
19. Nernst, W. Die theoretischen und experimentellen Grundlagen des neuen Wärmesatzes. *Annalen der Physik* **1918**, *362*, 395–412. https://doi.org/10.1002/andp.19183621202.
20. Vopson, M.M. The mass-energy-information equivalence principle. *AIP Advances* **2019**, *9*, 095206. https://doi.org/10.1063/1.5123794.
21. Landauer, R. Irreversibility and Heat Generation in the Computing Process. *IBM Journal of Research and Development* **1961**, *5*, 183–191. https://doi.org/10.1147/rd.53.0183.
22. Bekenstein, J.D. Black Holes and Entropy. *Physical Review D* **1973**, *7*, 2333–2346. https://doi.org/10.1103/PhysRevD.7.2333.
23. Hawking, S.W. Black hole explosions? *Nature* **1974**, *248*, 30–31. https://doi.org/10.1038/248030a0.
24. Wheeler, J.A. Geons. *Physical Review* **1955**, *97*, 511–536. https://doi.org/10.1103/PhysRev.97.511.
25. James, O.; von Tunzelmann, E.; Franklin, P.; Thorne, K.S. Gravitational lensing by spinning black holes in astrophysics, and in the movie Interstellar. *Classical and Quantum Gravity* **2015**, *32*, 065001. https://doi.org/10.1088/0264-9381/32/6/065001.
26. Bardeen, J.M. Timelike and null geodesics in the Kerr metric. In Proceedings of the Proceedings, Ecole d'été de Physique Théorique: Les Astres Occlus, Les Houches, France, 1973; pp. 215–240.

 doi:10.20944/preprints202507.1448.v8

27. Hioki, K.; Maeda, K.I. Measurement of the Kerr spin parameter by observation of a compact object's shadow. *Phys. Rev. D* **2009**, *80*, 024042. https://doi.org/10.1103/PhysRevD.80.024042.
28. Asada, K.; Nakamura, M. THE STRUCTURE OF THE M87 JET: A TRANSITION FROM PARABOLIC TO CONICAL STREAMLINES. *The Astrophysical Journal Letters* **2012**, *745*, L28. https://doi.org/10.1088/2041-8205/745/2/L28.
29. Nakamura, M.; Asada, K.; Hada, K.; Pu, H.Y.; Noble, S.; Tseng, C.; Toma, K.; Kino, M.; Nagai, H.; Takahashi, K.; et al. Parabolic Jets from the Spinning Black Hole in M87. *The Astrophysical Journal* **2018**, *868*, 146. https://doi.org/10.3847/1538-4357/aaeb2d.
30. Miyoshi, M.; Kato, Y.; Makino, J. The Jet and Resolved Features of the Central Supermassive Black Hole of M87 Observed with the Event Horizon Telescope (EHT). *The Astrophysical Journal* **2022**, *933*, 36. https://doi.org/10.3847/1538-4357/ac6ddb.
31. Nikonov, A.S.; Kovalev, Y.Y.; Kravchenko, E.V.; Pashchenko, I.N.; Lobanov, A.P. Properties of the jet in M87 revealed by its helical structure imaged with the VLBA at 8 and 15 GHz. *Monthly Notices of the Royal Astronomical Society* **2023**, *526*, 5949–5963. https://doi.org/10.1093/mnras/stad3061.
32. Kocherlakota, P.; Rezzolla, L.; Roy, R.; Wielgus, M. Hotspots and photon rings in spherically symmetric space–times. *Monthly Notices of the Royal Astronomical Society* **2024**, *531*, 3606–3641. https://doi.org/10.1093/mnras/stae1321.
33. Joshi, R.K.; Debnath, S.; Chattopadhyay, I. Shocks in Radiatively Driven Time-dependent, Relativistic Jets around Black Holes. *The Astrophysical Journal* **2022**, *933*, 75. https://doi.org/10.3847/1538-4357/ac70de.
34. Blandford, R.D.; Znajek, R.L. Electromagnetic extraction of energy from Kerr black holes. *Monthly Notices of the Royal Astronomical Society* **1977**, *179*, 433–456. https://doi.org/10.1093/mnras/179.3.433.
35. Merloni, A.; Fabian, A.C. Accretion disc coronae as magnetic reservoirs. *Monthly Notices of the Royal Astronomical Society* **2001**, *321*, 549–552. https://doi.org/10.1046/j.1365-8711.2001.04060.x.
36. Vincent, F.H.; Gralla, S.E.; Lupsasca, A.; Wielgus, M. Images and photon ring signatures of thick disks around black holes. *A&A* **2022**, *667*, A170. https://doi.org/10.1051/0004-6361/202244339.
37. Johnson, M.D.; Lupsasca, A.; Strominger, A.; Wong, G.N.; Hadar, S.; Kapec, D.; Narayan, R.; Chael, A.; Gammie, C.F.; Galison, P.; et al. Universal interferometric signatures of a black hole's photon ring. *Science Advances* **2020**, *6*, eaaz1310. arXiv:1907.04329, https://doi.org/10.1126/sciadv.aaz1310.
38. Farrah, D.; et al. A Preferential Growth Channel for Supermassive Black Holes in Elliptical Galaxies at $z < 2$. *The Astrophysical Journal* **2023**, *943*, 133. https://doi.org/10.3847/1538-4357/aca6e1.
39. Croker, K.S.; Farrah, D.; et al. DESI Dark Energy Time Evolution is Recovered by Cosmologically Coupled Black Holes. *Journal of Cosmology and Astroparticle Physics* **2024**, *2024*, 094. https://doi.org/10.1088/1475-7516/2024/10/094.
40. Wheeler, J.A. Information, Physics, Quantum: The Search for Links. In *Complexity, Entropy, and the Physics of Information*; Zurek, W.H., Ed.; Addison-Wesley: Redwood City, CA, 1990; Vol. 8, *Santa Fe Institute Studies in the Sciences of Complexity*, pp. 3–28.